Direct Assimilation of Radar Reflectivity Data Using 3DVAR: Treatment of Hydrometeor Background Errors and OSSE Tests

CHENGSI LIU

Center for Analysis and Prediction of Storms, University of Oklahoma, Norman, Oklahoma

MING XUE

Center for Analysis and Prediction of Storms, and School of Meteorology, University of Oklahoma, Norman, Oklahoma

RONG KONG

School of Meteorology, University of Oklahoma, Norman, Oklahoma

(Manuscript received 25 January 2018, in final form 7 November 2018)

ABSTRACT

Despite the well-known importance of background error covariance in data assimilation, not much study has been focused on its impact on the assimilation of radar reflectivity within a three-dimensional variational (3DVar) framework. In this study, it is shown that unphysical analysis increments of hydrometeors are produced when using vertically homogeneous background error variance. This issue cannot be fully solved by using the so-called hydrometeor classification in the reflectivity observation operator. Alternatively, temperature-dependent background error profiles for hydrometeor control variables are proposed. With such a treatment, the vertical background error profiles are specified to be temperature dependent, allowing for more physical partitioning of radar-observed precipitation information among the liquid and ice hydrometeors. The 3DVar analyses using our treatment are compared with those using constant background error or ''hydrometeor classification'' through observing system simulation experiments with a simulated supercell storm. Results show that 1) 3DVar with constant hydrometeor background errors produces unphysical rainwater at the high levels and unphysical snow at the low levels; 2) the hydrometeor classification approach reduces unphysical rainwater and snow at those levels, but the analysis increments are still unphysically spread in the vertical by the background error covariance when the vertically invariant background errors are used; and 3) the temperature-dependent background error profiles enable physically more reasonable analyses of liquid and ice hydrometeors from reflectivity assimilation.

1. Introduction

Although much progress has been made in the area of convective-scale data assimilation (DA) and numerical weather prediction (NWP), obtaining accurate initial conditions for convective-scale NWP remains a major challenge. A major issue for convective-scale DA is the lack of sufficient and direct observations within thunderstorms and their environment. Radar reflectivity data, which have higher spatial and temporal resolutions than conventional observations and contain hydrometeor information, are the most important data for convective-scale DA. Complex cloud analysis (Hu et al. 2006), ensemble Kalman filter (EnKF) (e.g., Tong and Xue 2005), and 3D variational (3DVar) (Gao and Stensrud 2012) DA methods are currently the three main types of methods for assimilating radar reflectivity for convective-scale models that contain ice microphysics, while 4D variational (4DVar) method has mainly be used with the assumptions of warm rain microphysics (e.g., Sun and Crook 1997).

Complex cloud analysis schemes adjust thermodynamic and hydrometeor variables based on radar reflectivity data, satellite, and surface observations, etc. (Albers et al. 1996). Cloud analysis is generally computationally fast and relatively easy to implement, and has been shown to enable the buildup of reasonable 3D cloud structures and precipitation fields and quite effectively alleviate the precipitation spinup problem (Hu et al. 2006; Kain et al. 2010; Sun et al. 2014; Xue et al. 2003). However, cloud analysis algorithms typically rely

Corresponding author: Ming Xue, mxue@ou.edu

DOI: 10.1175/MWR-D-18-0033.1

on empirical relationships that have many uncertainties. Moreover, such methods do not utilize background and observation error information, and hence cannot obtain statistically optimal estimations.

Variational methods can also be used to assimilate reflectivity data; optimal analyses are obtained by minimizing a cost function in which the contributions of the background and observations are weighted by their respective error covariances. Four-dimensional variational (4DVar) method uses the forecast model as a strong constraint in the cost function so that the analysis can be consistent with the forecast model. For the convective scale, the microphysical processes are important and complex ice microphysics schemes are highly nonlinear, which creates many practical issues that are difficult to overcome (Xu 1996), like nonlinearity associated with the highly nonlinear physics. For this reason, existing 4DVar systems that assimilate radar reflectivity data generally assume warm rain microphysics and convert reflectivity to rainwater mixing ratio before assimilation (Sun and Crook 1997; Wang et al. 2013b).

EnKF uses an ensemble of forecasts to estimate the background error covariances. Not requiring tangent linear or adjoint models of the observation operators, EnKF can more easily use nonlinear observation operators (e.g., of radar reflectivity) and models with complex ice microphysics. The ability of EnKF to assimilate radar data has been shown by many studies (Aksoy et al. 2009, 2010; Jung et al. 2008a,b; Tong and Xue 2005; Xue et al. 2006). While EnKF can estimate a flow-dependent background error covariance, the estimated covariance matrix is often severely affected by the sampling and model errors (Houtekamer and Mitchell 1998; Houtekamer et al. 2009). The hybrid method, which combines the use of ensemble-derived flow-dependent background error covariance with static covariance within a variational framework, requires the capability of variationally assimilating reflectivity data (Hamill and Snyder 2000; Kong et al. 2018).

Apart from being needed for constructing a hybrid DA system, using 3DVar to assimilate radar data is also more practical because of its relatively low computational cost. In the MM5 and later WRF 3DVar systems, Xiao et al. (2007) proposed a procedure to directly assimilate reflectivity although only the liquid phase of hydrometeors was considered, to simplify the problem. The more recent implementation of reflectivity assimilation within WRF variational DA systems retrieves hydrometeor mixing ratios prior to assimilation (Wang et al. 2013a).

When considering ice microphysics in the absence of model constraint (either in the form of a strong constraint as in 4DVar or in the form of ensemble error covariances), 3DVar usually has difficulties in properly partitioning radar-observed precipitation information among multiple hydrometeors, and often produces unphysical analyses of hydrometeors. For example, rainwater can be placed way above the freezing level even without strong updraft while snow may be erroneously analyzed way below the melting level. One approach to avoid this problem is to modify the reflectivity observation operator so that it is temperature dependent. In Gao and Stensrud (2012), reflectivity is made to be a function of rainwater only below the 5°C level, and a function of snow and hail only above the −5°C level. Between these two levels, the equivalent reflectivity is made to be a weighted average of the contributions from liquid and ice hydrometeor species, with the weights being linearly dependent on temperature. This approach is called "hydrometeor classification" by Gao and Stensrud (2012).

One of the problems with the hydrometeor classification approach is the effective disallowance of hail at levels below 5°C. On the other hand, when the background error variances of the hydrometeors are assumed to be vertically invariant, as is the case in Gao and Stensrud (2012), unphysical analysis increments of hydrometeors can be produced by their vertical spreading through background error covariance. In addition, with the formula used by Gao and Stensrud (2012), at 0°C temperature, the contributions of liquid and ice hydrometeors to the equivalent reflectivity are unphysically halved.

In ensemble-based DA system, because of the use of flow-dependent background error covariance, the hydrometeors analyses will be physically consistent with the forecast model, and the hydrometeor classification approach would not be necessary. When the 3DVar framework is used to construct an ensemble–variational hybrid system (Kong et al. 2018), it is also preferred that the reflectivity operator used in the hybrid system is the same as that used in the coupling EnKF system; in other words, ad hoc modification to the observational operator in the hydrometeor classification approach is undesirable.

In this study, we propose an alternative approach to deal with the 3DVar reflectivity assimilation problem discussed above. As opposed to using spatially uniform errors as in Gao and Stensrud (2012), our new approach introduces additional information or constraint to the analysis system by defining temperature-dependent background error covariances for the hydrometeor variables. The impact of the temperature-dependent error profiles on the 3DVar analyses of a supercell storm is examined through observing system simulation experiments (OSSEs), by comparing the results with those using the constant error profiles with or without the hydrometeor classification treatment.

This paper is organized as follows: in section 2, the proposed temperature-dependent background error

profiles for the hydrometeor variables are described. The design of three 3DVar experiments, which use, respectively, the proposed background error profiles, constant error profiles with and without the hydrometeor classification, is presented in section 3. In section 4, we compare the OSSE results from the three experiments. Conclusions are given in section 5.

2. Temperature-dependent background error profiles

In the Advance Regional Prediction System (ARPS) 3DVar system (Gao et al. 2004; Xue et al. 2003), the default background error variances for hydrometeor mixing ratios are assumed to be homogeneous. With such error variances, unphysical analysis increments, such as rainwater at the upper levels and snow far below the freezing level, can be produced. To avoid the unphysical hydrometeor analysis increments, the so-called hydrometeor classification algorithm was proposed in Gao and Stensrud (2012), in which the original reflectivity observation operator based on Lin et al. (1983) was modified to be temperature dependent.

The reflectivity factor Z can be simulated based on model mixing ratios of rainwater q_r, snow q_s, and hail q_h, following Tong and Xue (2005):

$$Z = 10\log_{10}(Z_e), \tag{1}$$

$$Z_e = Z_{er}(q_r) + Z_{es}(q_s) + Z_{eh}(q_h), \tag{2}$$

where Z_{er}, Z_{es}, and Z_{eh} are the contributions to equivalent reflectivity Z_e by rainwater, snow, and hail, respectively.

The equivalent reflectivity factors contributed by rainwater is calculated, based on Smith et al. (1975), from

$$Z_{er} = \frac{10^{18}\times 720(\rho q_r)^{1.75}}{\pi^{1.75}N_r^{0.75}\rho_r^{1.75}} = 3.63\times 10^9\times(\rho q_r)^{1.75}, \tag{3}$$

where $\rho_r = 1000\,\mathrm{kg\,m^{-3}}$ is the density of rainwater and ρ (in $\mathrm{kg\,m^{-3}}$) is the density of air; and $N_r = 8.0\times 10^6\,\mathrm{m^{-4}}$ is the intercept parameter in the assumed Marshall–Palmer exponential raindrop size distribution.

If the temperature is less than 0°C, the component of reflectivity for dry snow is

$$Z_{es} = \frac{10^{18}\times 720K_i^2\rho_s^{0.25}(\rho q_s)^{1.75}}{\pi^{1.75}K_r^2N_s^{0.75}\rho_i^2} = 9.80\times 10^8\times(\rho q_s)^{1.75}. \tag{4}$$

Here $\rho_s = 1000\,\mathrm{kg\,m^{-3}}$ is the density of snow and $\rho_i = 917\,\mathrm{kg\,m^{-3}}$ is the density of ice, $N_s = 3.0\times 10^6\,\mathrm{m^{-4}}$ is the intercept parameter for snow, and $K_i^2 = 0.176$ is the dielectric factor for ice while $K_r^2 = 0.93$ is the same for water. Wet snow, which occurs at temperatures higher than 0°C, is treated in a similar way as rainwater, and the equivalent reflectivity factor-mixing ratio relation is

$$Z_{es} = \frac{10^{18}\times 720(\rho q_s)^{1.75}}{\pi^{1.75}N_s^{0.75}\rho_s^{1.75}} = 4.26\times 10^{11}\times(\rho q_s)^{1.75}. \tag{5}$$

For hail, the wet hail formulation of Smith et al. (1975) is used:

$$Z_{eh} = \left(\frac{10^{18}\times 720}{\pi^{1.75}N_h^{0.75}\rho_h^{1.75}}\right)^{0.95}(\rho q_h)^{1.6625} = 4.33\times 10^{10}\times(\rho q_h)^{1.66}, \tag{6}$$

where $\rho_h = 913\,\mathrm{kg\,m^{-3}}$ is the density of hail. The hail intercept parameter of $N_h = 4.0\times 10^4\,\mathrm{m^{-4}}$ is used, which is slightly larger than that used in Smith et al. (1975), implying more occurrences of hail at smaller sizes.

Based on the consideration that rainwater should generally exist below the freezing level, and snow and hail should generally exist above the freezing level, the reflectivity operator is modified to the following form in Gao and Stensrud (2012):

$$Z = \begin{cases} 10\log_{10}Z_{er} & T_b \ge 5^\circ\mathrm{C} \\ 10\log_{10}(Z_{es}+Z_{eh}) & T_b \le -5^\circ\mathrm{C} \\ 10\log_{10}[\alpha Z_{er} + (1-\alpha)(Z_{es}+Z_{eh})] & -5^\circ > T_b > 5^\circ\mathrm{C}, \end{cases} \tag{7}$$

where T_b is the background temperature in Celsius, and weighting coefficient a varies linearly between 0 and 1 as a function of temperature ranging between −5° and 5°C. With this modified reflectivity observation operator, the sensitivity of reflectivity to snow and hail below the 5°C level, and that to rainwater above the −5°C level are disallowed. As a result, in the absence of background error correlation, the assimilation of reflectivity will not generate rainwater above the −5°C level, or snow and hail below the 5°C level. If homogeneous background error covariance is used, however, as in the default scheme of ARPS 3DVar, undesirable hydrometers at

these levels will appear. Moreover, the above treatment does not consider the situation of hail falling below the freezing level.

Another problem using the modified observation operator with the homogenous background error covariance is that the reflectivity data assimilation will be unable to remove spurious rainwater in the background at the upper levels, and more importantly unable to remove spurious snow and hail at the lower levels when assimilating reflectivity data because the 3DVar system cannot detect such spurious hydrometeors since they do not appear in the reflectivity observation operator. As pointed out earlier, in the transition zone between −5° and 5°C, the equivalent reflectivity contributions from coexisting liquid and ice phases are excessively reduced, and in fact, to half of the correct values at 0°C.

Our proposed solution to the problem is, as mentioned earlier, to define temperature-dependent background error profiles for the hydrometeor variables. For each of the profiles, the errors are defined separately in three vertical sections divided by temperature thresholds. The error values in the top and bottom sections are still constant but in different magnitudes. The value in the middle sections increases or decreases from the bottom-section value to the top-section value based on a hyperbolic tangent function, according to

$$E = \begin{cases} E_h & T < T_h \\ (E_h + E_l)/2 - \dfrac{(E_h - E_l)}{2 \times \tanh(2\alpha)} \tanh\left[\dfrac{2\alpha}{1-a}(i-a)\right] & T_h \le T \le T_l \\ E_l & T > T_l \end{cases}, \tag{8}$$

where E is the background error magnitude and T the temperature. The variables E_h and E_l are constant errors for the high and low levels with temperature smaller than T_h and greater than T_l, respectively. Here i is the temperature of certain level in the transition zone and n is the temperature difference between the high level and low level. The variable "a" is equal to $(1+ n)/2$ and α is a tuning parameter that can be a value between 0.2 and 5.0, and is set as 1.0 in this paper. In real data assimilation experiments, the background error profiles can be determined statistically using data from precipitating columns (e.g., with a form of the NMC method; Parrish and Derber 1992). In our idealized experiments presented in this paper, the error magnitudes at the high and low levels are estimated by the root-mean-square errors (RMSEs) with the mean calculated over all the cycles in the OSSEs. For rainwater, T_h and T_l, are set as −5° and 5°C, respectively, while for snow and hail, they are set as −30° and 5°C, respectively. The lower temperature of the upper threshold helps prevent discontinuity that can appear in the analysis increments of snow and hail. The parameters in Eq. (8) used in this study are given in Table 1 and the error profiles are shown in Fig. 1.

3. Experimental design

In this study, a classic supercell storm that occurred on 20 May 1977 in Del City, Oklahoma, is simulated using the ARPS model (Xue et al. 2001) to serve as a truth simulation of the OSSEs. The domain size is 35 × 35 × 35, with 2 km horizontal and 0.5 km vertical grid spacings. The environment of the supercell is defined by a modified real sounding while the truth storm simulation is initialized by a thermal bubble. More information about the truth simulation can be found in Tong and Xue (2005).

The simulated radial velocity V_r and reflectivity Z are produced by a pseudoradar located at the southwest corner of the model domain. The radial velocity operator based on the model velocity is written as

$$V_r = u \sin\phi \cos\mu + v \cos\phi \cos\mu + w \sin\mu, \tag{9}$$

where μ and ϕ are the elevation and azimuth angles of radar beams, respectively; and u, v, and w are the model-simulated velocities interpolated to the scalar grid points.

Random noise is added to the simulated V_r and Z observations given by Eqs. (9) and (1), respectively. The noise is sampled from Gaussian distributions with zero mean and standard deviations of $1\,\mathrm{m\,s^{-1}}$ for V_r and 3 dBZ for Z. Both radial velocity and reflectivity observations are assimilated by the ARPS 3DVar at 5-min intervals in the 1-h DA window. The first analysis is performed at 25 min of the truth simulation. Similar to Kong et al. (2018), the initial background is the ensemble mean of the 5-min ensemble forecasts initiated from the ensemble perturbations valid at the 20-min of the truth simulation. The background error decorrelation scales are 3.5 km in the horizontal and 1.1 km in the vertical for all analysis variables, based on the optimal scales obtained in Kong et al. (2018) for similarly configured 3DVar OSSEs. To help suppress spurious reflectivity in the background, clear-air reflectivity is also assimilated (Tong and Xue 2005).

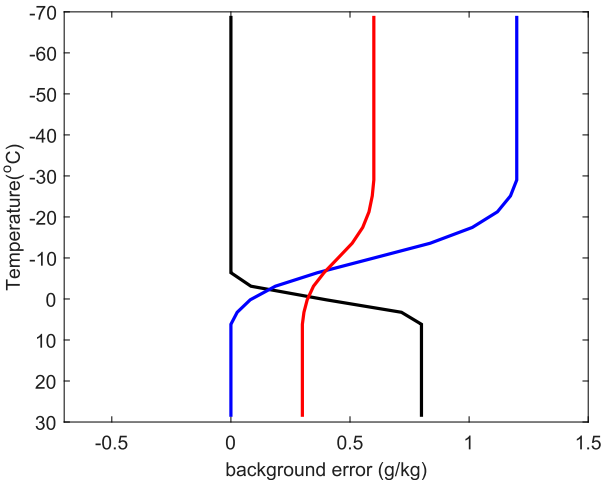

FIG. 1. The temperature-dependent background error profiles of the mixing ratio of rainwater (black), snow (blue), and hail (red).

Three experiments are conducted using 3DVar with 1) the invariant background error profiles (CTRL), 2) the invariant background error profiles and hydrometeor classification in the reflectivity observation operator (3DVarHC), and 3) the new temperature-dependent background error profile (3DVarTD). Another experiment, 3DVarHCS, which is the same as 3DVarHC, except that a much smaller vertical background error decorrelation scale (100 m) is used. The experiment results are presented in the next section.

4. Experimental results

a. *Results of the first analysis*

1) COMPARISON OF TOTAL REFLECTIVITY ANALYSES

Figure 2 shows the reflectivity and wind vector fields in an east–west vertical cross section through the maximum vertical velocity of the simulated truth storm at the time of first analysis (25 min), from the truth simulation, background, and three DA experiments. Compared with the simulated truth, the reflectivity in the background is weak and has a wide horizontal coverage unlike that of a deep convective cell. Also, there is some spurious reflectivity away from the main storm. After the first assimilation of radar data, the analyzed reflectivity fields in CTRL, 3DVarHC, and 3DVarTD are much closer to the truth, and the spurious reflectivity in the east of the main storm is partly suppressed. However, the intensity of the reflectivity core is more underestimated in all three analyses, and the vertical motion in the main storm region is still mostly downward. Some new spurious reflectivity is also produced in supposedly clear air regions. It is a known problem of direct variational assimilation of reflectivity that large gradients of cost function can be produced in areas of small background hydrometeor mixing ratios, which prevents efficient minimization convergence (Sun and Crook 1997). Figure 2 also shows that the vertical velocity is not properly analyzed within the updraft region. In the ARPS 3DVAR system whose static background error does not contain cross covariance between wind and hydrometeor fields, the wind field can only be updated by the radial velocity data. We have found that when using hydrometeor mixing ratios as the control variables and when analyzing reflectivity and radial velocity data simultaneously, the assimilation of radial velocity data is ineffective, and special treatments are needed to circumvent this problem, which will be discussed in a separate paper. Because of the focus on reflectivity assimilation in this paper, this issue is unimportant for this study. Through the assimilation cycles, rather accurate vertical velocity does develop later on (not shown).

TABLE 1. The parameters in the background error profiles for rainwater, snow, and hail mixing ratios.

	q_r	q_s	q_h
T_h (°C)	−5	−30	−30
T_l (°C)	5	5	5
E_h (g kg^{-1})	0	1.2	0.6
E_l (g kg^{-1})	0.8	0	0.3

Figure 2 also indicates that the reflectivity analyses from CTRL, 3DVarHC, and 3DVarTD are generally similar. Since both the hydrometeor classification and temperature-dependent background error profiles aim to better partition the radar-observed precipitation information among the hydrometeors, and the cost function minimization tries to minimize the simulated reflectivity from observed values, the analyzed reflectivity is expected to be relatively close to the observed reflectivity values. The key is in the accuracy of the analyzed hydrometeor fields, which are not directly observed.

2) COMPARISON OF ANALYZED HYDROMETEOR FIELDS

When multiple hydrometeors species contribute to the reflectivity, and only reflectivity is observed, the problem of directly assimilating reflectivity data for the purpose of determining several hydrometeor variables is underdetermined. Therefore, even if the analyzed total reflectivity fits well to its observations, the individual hydrometeor fields may not be correctly analyzed. The hydrometeor classification treatment of Gao and Stensrud (2012), and our use of temperature-dependent background errors both try to introduce additional constraints into the 3DVar system. To evaluate

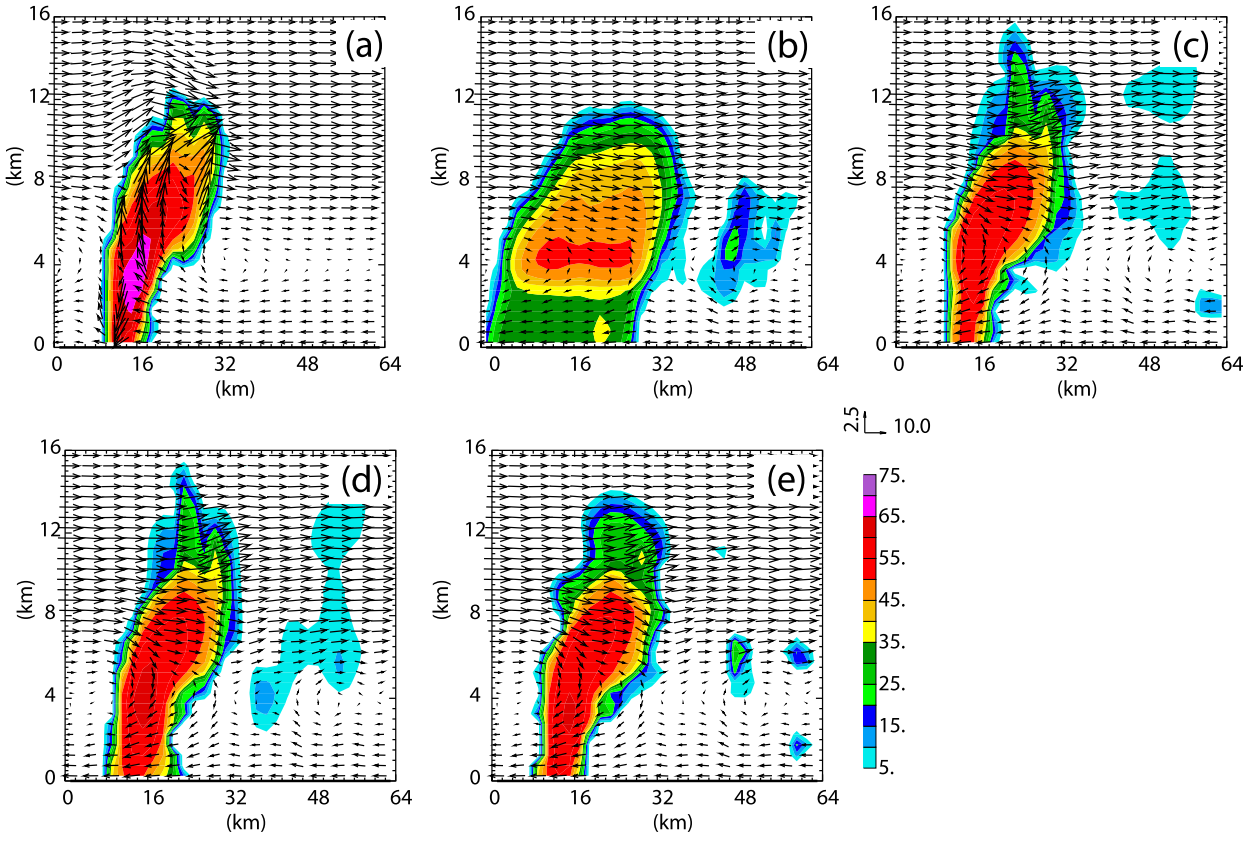

FIG. 2. The reflectivity (shading) and wind vectors in a vertical cross section through the maximum vertical velocity of simulated truth storm at the time of first analysis (25 min), for (a) the truth simulation, (b) the background, (c) the CTRL, (d) 3DVarHC, and (e) 3DVarTD experiments.

the true quality of analyses, the analyzed rainwater, snow, and hail mixing ratio fields, and their corresponding contributions to reflectivity (in dBZ) are shown in Fig. 3. The contributions of rainwater Z_r, snow Z_s, or hail Z_h are defined as the logarithmic equivalent reflectivity from the individual hydrometeors [e.g., $Z_r = \log_{10}(Z_{er})$].

In the truth simulation, nonzero rainwater (snow) mixing ratio mainly exists below (above) the melting level (which is roughly at a 4-km height), as shown in Figs. 3a and 3b. For hail (Fig. 3c), there are significant hailstones blow 5 km and the magnitude of low-level Z_h is over 65 dBZ because hailstones can reach the ground before fully melted. While hail below the 5°C level is ignored by the hydrometeor classification scheme according to Eq. (7), it is allowed when using the temperature-dependent background error profiles defined in Eq. (8).

In the forecast background (Figs. 3d–f), because the storm is much weaker than the truth, the hydrometeor mixing ratios are also much less. In the background, little hail is shown below the freezing level (Fig. 3f), while rainwater (snow) exists only below (above) the freezing level (Figs. 3d and 3e).

(i) Analyzed hydrometeor fields from CTRL

With the assimilation of radar data (mainly of reflectivity data that have direct impact on the hydrometeor fields in the first analysis, while the effects of V_r data assimilation have to be accumulated through 3DVar DA cycles), the analyzed hydrometeor distributions in CTRL become narrower than in the background, and closer to the truth (Figs. 3g–i); the magnitudes are also much increased. However, the partitioning of reflectivity observation information across the hydrometeors is not quite right. In Fig. 3h, snow mixing ratio and corresponding reflectivity below the melting level are much larger than those above the melting level, which is obviously unphysical. The values at the lower levels are apparently large because the coefficient of the equivalent reflectivity equation for wet snow [4.26×10^{11} in the Eq. (5)] is much larger than that for dry snow [9.80×10^{8} in the Eq. (4)]. The larger the coefficient in the Z_e equation is, the more sensitive Z_e is to the corresponding hydrometeor mixing ratio, where the adjoint sensitivity is the gradient of Z_e with respect to the mixing ratio. Because variational minimization tends to adjust most

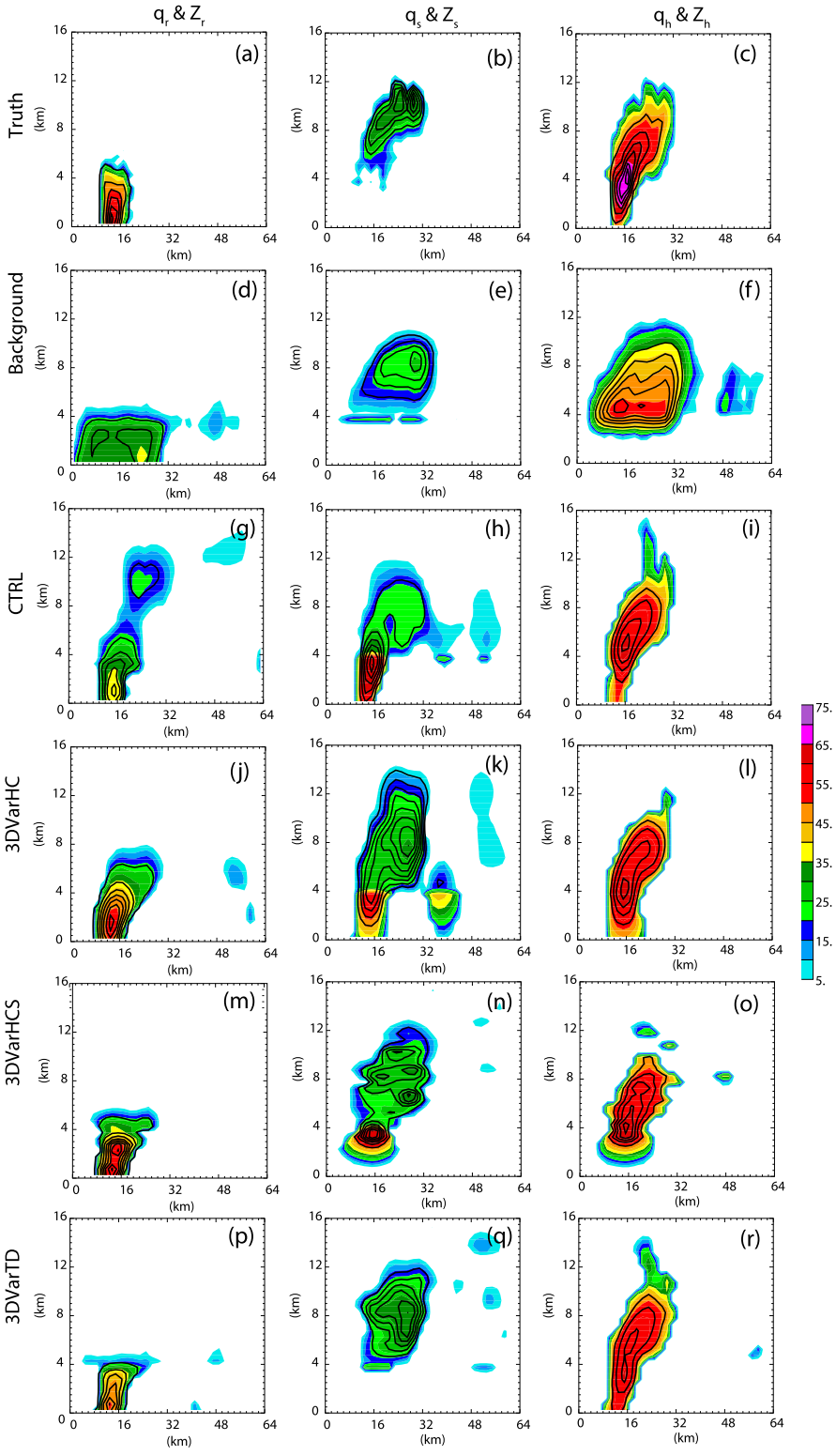

FIG. 3. The (left) rainwater, (middle) snow, and (right) hail mixing ratios (contours starting at 0.5 g kg^{-1} and at intervals of 0.5 g kg^{-1}) and corresponding reflectivity (shading) in a vertical cross section through the maximum vertical velocity of simulated truth storm at the first analysis time for the (a)–(c) truth simulation, (d)–(f) background, (g)–(i) CTRL, (j)–(l) 3DVarHC, (m)–(o) 3DVarHCS, and (p)–(r) 3DVarTD.

sensitive variables the most (e.g., using algorithms having properties of steepest descent), the adjustment to snow mixing ratio below the freezing level (where snow is expected to be wet) will be much larger than to snow above the freezing level, leading to much more snow mixing ratio at the lower levels (Fig. 3h).

Since the same background error of $0.6\,g\,kg^{-1}$ is used for all hydrometeor mixing ratios in CTRL, the partition of the reflectivity observation information is almost exclusively controlled by the sensitivity to (gradient with respect to) the hydrometeors in the reflectivity observation operator. Below the melting level, because the reflectivity in the operator is most sensitive to wet snow, the analyzed reflectivity component from snow is the largest in CTRL (Fig. 3h); however, such large values below the freezing level do not exist in the true simulation at all (Fig. 3b). Above the melting level, some unphysical analysis increments of rainwater are also found (Fig. 3g). In Fig. 3i, some hail analysis increments are found at the low levels but the values in the truth simulation are much larger; this is because most of the adjustment had been made to snow at the lower level, resulting in too small adjustments to hail mixing ratio.

(ii) Analyzed hydrometeor fields from 3DVarHC

In the hydrometeor classification version of the reflectivity observation operator, contributions of ice hydrometeors below the 5°C level and rainwater above the −5°C level are excluded, so that they cannot be directly produced by the reflectivity observation within the 3DVar analysis. Compared with the CTRL analysis below the melting level (Fig. 3g), rainwater mixing ratio from 3DVarHC is much larger (Fig. 3j) because only rainwater is included in the reflectivity operator at those levels. Similarly, the snow analysis increment at the upper levels is increased more than in CTRL because of the absence of competition from rainwater (Fig. 3k). Figure 3k also shows that the large unphysical snow increments at the low levels in CTRL are greatly suppressed because of the lack of a direct link to snow in the reflectivity operator at those levels, but snow below the melting level is still significantly overestimated. The unphysical rainwater increment at the high levels in CTRL is correctly suppressed (Fig. 3j).

However, if we compare the analyzed rainwater and snow fields in 3DVarHC with the truth fields in more details, we still notice unphysical spreading of rainwater above the freezing level (Fig. 3j), and unphysical spreading of snow below the freezing level, some of which even reaches the ground (Fig. 3k). Another issue with hydrometeor classification is the exclusion of hail below the 5°C level, which results in a small analysis increment at the low levels for hail produced only by the vertical spreading via the background error correlation (Fig. 3l).

One way to reduce the unphysical vertical spreading of hydrometeor analysis increments is to adjust the vertical background error decorrelation scale. This is done in experiment 3DVarHCS where the vertical scale is reduced from 1.1 km to 100 m. The 100 m is smaller than the vertical grid spacing of 500 m in our experiment; therefore, vertical spreading should be virtually eliminated. This choice of a very small decorrelation scale is mainly for the purpose of illustrating the effects of vertical increment spreading.

With the 100-m vertical decorrelation scale, the unphysical vertical spreading of analysis increments is much reduced; for example, there is no wet snow below 2 km in 3DVarHCS (Fig. 3n). However, within regions of storms, there should be vertical error correlations where updrafts and downdrafts are deep and strong (see, e.g., Tong and Xue 2005). Kong et al. (2018) found via OSSEs that the optimal vertical decorrelation scale for 3DVar for this case should be about 1 km. The vertical decorrelation scale of 100 m in this experiment is obviously too short to obtain optimal analyses. Moreover, the issue of significantly overestimating snow in the melting layer still exists in 3DVarHCS (Fig. 3n) because of very large sensitivity to wet snow in the melting layer; the hydrometeor classification treatment dose not eliminate this issue.

(iii) Analyzed hydrometeor fields from 3DVarTD

In the temperature-dependent background error profiles, the background error of snow below the 5°C level and of rainwater above the −5°C level are set to zero, which means that the analysis system will very much trust the background. This is obviously based on physical conditions. When error statistics are obtained from model-predicted fields, similar temperature dependences are expected, although the actual statistical distribution is left for future studies. With this setting of 3DVarTD, nonphysical analysis increments of snow (rainwater) below (above) the melting level are no longer produced (Figs. 3q and 3p). Because the physical constraint is considered via background error covariance profiles, proper vertical spreading of hydrometeor analysis increments can be taken into account via vertical variations of the error magnitudes.

In CTRL, 3DVarHC, and 3DVarHCS, wet snow is significantly overestimated below the melting level (Figs. 3h, 3k, and 3n) because the cost function sensitivity to snow is large where the snow is expected to be wet. In contrast, the background error variance of snow is much smaller below the melting level in 3DVarTD (see Fig. 1) so that the analysis increment of wet snow is

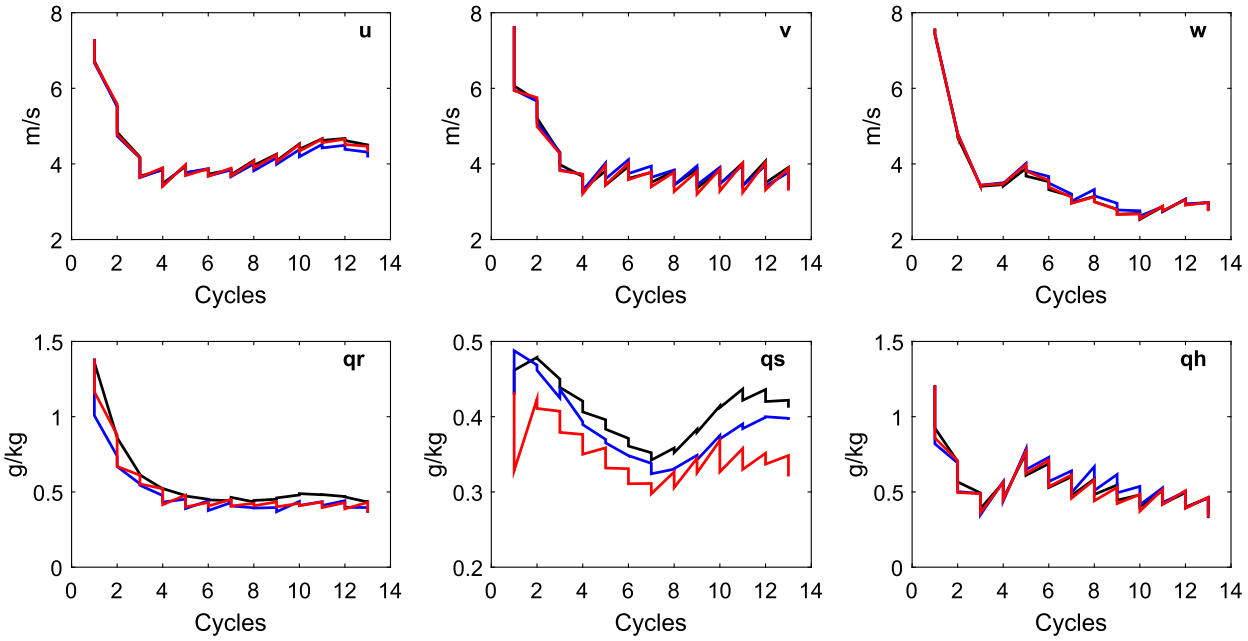

FIG. 4. The RMSEs of analyses and forecasts during the DA cycles for CTRL (black), 3DVarHC (blue), and 3DVarTD (red), for different state variables as labeled.

much smaller (Fig. 3q), alleviating the overestimation problem.

For hail, significant magnitudes of analysis increments are found below the melting level (Fig. 3r), much closer to the truth than in other experiments; this is attributed to the fact that hail and its error variance is considered in the background error profile of hail (Fig. 1).

Overall, the spatial patterns and magnitudes of the analyzed rainwater, snow, and hail mixing ratios and corresponding reflectivity fields are much better reproduced by the single-time 3DVar analysis using our proposed background error profiles than those using a homogeneous error covariance. While the analyses using the hydrometeor classification observation operator are improved over CTRL, some issues are still shown. Given that only a single time analysis is performed, the analyzed hydrometeor fields are generally weaker than the truth, which is expected.

b. Results of cycled analyses

The previous section presents the results from the first data assimilation cycle. What we also want to know is the quality of the analyses and forecasts through the rest of the DA cycles when the storm structures are more accurately established. For this purpose, we examine the errors of the analysis and forecast hydrometeor fields in all DA cycles, and the fields at the end of the cycles.

The RMSEs of the wind components and hydrometeor mixing ratios are calculated in regions where reflectivity exceeds 10 dBZ in the true simulation. As shown in Fig. 4, the RMSEs of all experiments generally decrease with the forecast–analysis cycle. In addition, the RMSEs from the three experiments are very close except for the snow mixing ratio. The RMSEs of snow mixing ratio from 3DVarTD are lower than those of CTRL and 3DVarHC. Moreover, the analysis RMSEs of CTRL and 3DVarHC at the first analysis time are actually increased by the data assimilation, mainly because unphysical snow increments are created at the lower levels as discussed earlier and shown in Figs. 3h and 3k.

To further examine the differences in the analyzed hydrometeor fields from CTRL, 3DVarHC, and 3DVarTD after 1 h of DA cycles, the rainwater, snow, and hail mixing ratios and the corresponding reflectivity components at the last cycle are shown in Fig. 5 in a vertical cross section through the maximum vertical velocity of the truth simulation. Like the first time analyses discussed in section 4a, the unphysical snow mixing ratio at the low levels and the unphysical rainwater mixing ratio at the high levels are still shown in the analyses of CTRL and 3DVarHC after 1 h of DA cycles.

Figure 5a shows that the rainwater in the truth simulation can reach above 7 km because of the strong updraft in the storm. The rainwater analyses in both CTRL and 3DVarTD are much weaker than that of truth simulation while 3DVarHC has better rainwater intensity analysis since snow and hail are excluded in the

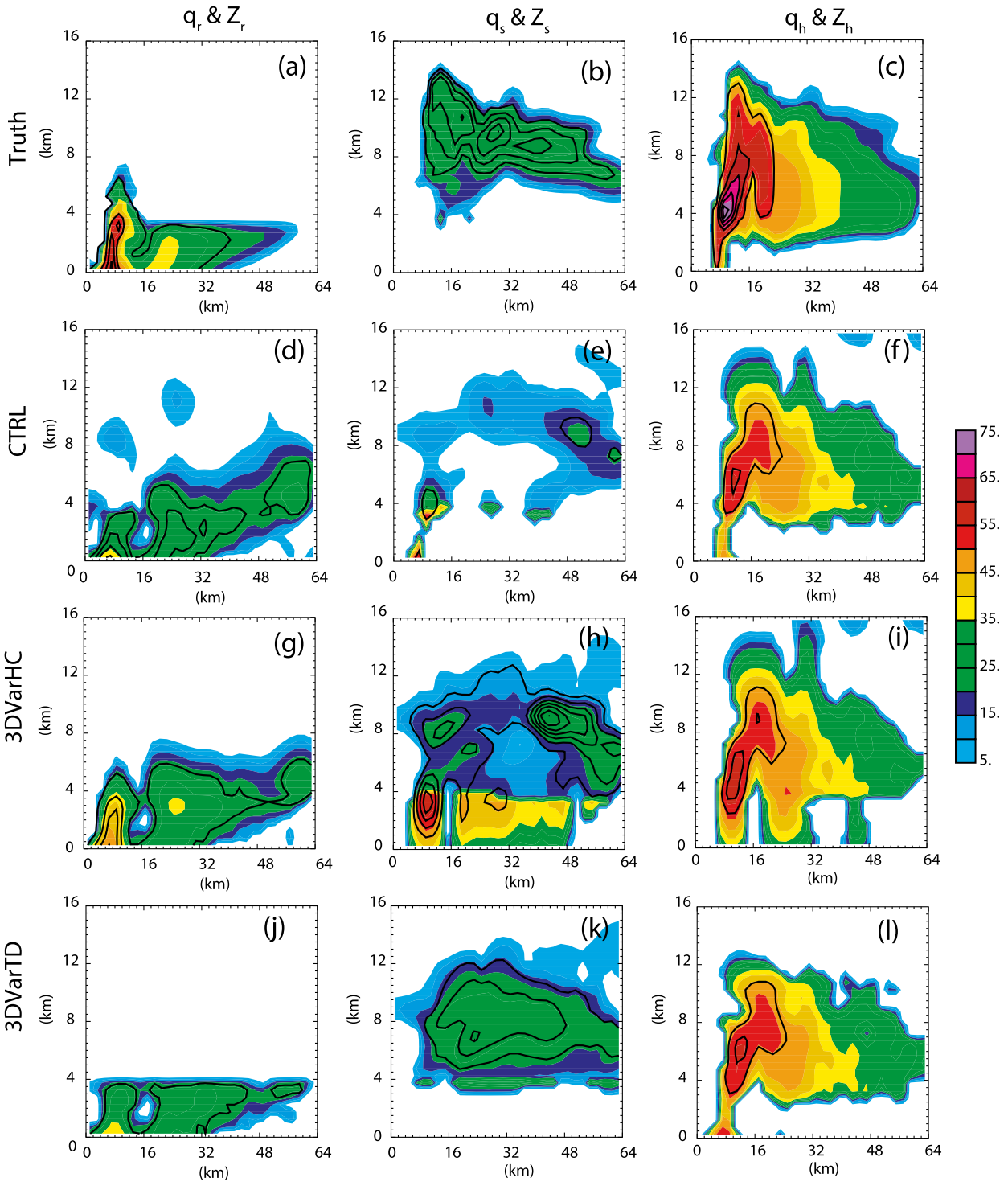

FIG. 5. The (left) rainwater, (middle) snow, and (right) hail mixing ratios (contours starting at 0.5 g kg^{-1} and at intervals of 0.5 g kg^{-1}) and the corresponding reflectivity (shading) in a vertical cross section through the maximum vertical velocity of the simulated truth storm at the end of DA cycles (from top to bottom) for the (a)–(c) truth simulation, (d)–(f) CTRL, (g)–(i) 3DVarHC, and (j)–(l) 3DVarTD.

reflectivity operator at the lower levels (Figs. 5d, 5g, and 5j). Because the background error of rainwater above the freezing level is set to zero, no rainwater analysis increment above the freezing level can be directly produced in 3DVarTD. Further tuning to the rainwater error profile can be made, by allowing some rainwater error above the freezing level. The presence of supercooled liquid water does depend on the updraft intensity, which could be accounted for by flow-dependent background error covariance from ensemble forecasts in a hybrid system developed recently for ARPS 3DVar (Kong et al. 2018). The snow analysis at the high levels of CTRL is clearly underestimated (Fig. 5e) while the unphysical wet snow at the low levels of 3DVarHC (Fig. 5h) becomes more prominent than that of the first analysis. For 3DVarTD, the snow analysis at the high levels (Fig. 5k) is slightly underestimated but no unphysical wet snow at the low levels is produced. For hail analysis in 3DVarHC (Fig. 5i), there are spurious hail below the overhanging reflectivity anvil at the low levels, which is apparently due to inappropriate analysis increment spreading associated with the constant background error variance and vertical spatial correlation. It is noted that the reflectivity core at the low levels in 3DVarTD is still underestimated even after DA cycling. We have found that this is because the gradient of the cost function is much smaller (larger) where background reflectivity is large (small) so that the hydrometeors near the reflectivity core are not sufficiently adjusted by observations, especially when clear-air reflectivity is assimilated. This issue is related to the nonlinearity of the reflectivity operator, and separate treatments to alleviate this problem will be the topic of a separate paper.

Overall, the analyzed hydrometeor fields at the end of the 1-h radar DA cycles remain the most accurate and physical in the experiment that uses our proposed temperature-dependent background error profiles for the hydrometeors. Issues found in the first 3DVar analysis with the hydrometeor classification treatment and with the constant background errors remain at the end of the 1-h DA cycles.

5. Summary and conclusions

To effectively and directly assimilate radar data, especially radar reflectivity data, using ARPS 3DVar, temperature-dependent background error profiles are proposed for the hydrometeor state variables associated with liquid- and ice-phase microphysics to better partition radar-observed precipitation information among hydrometeors. The proposed method is compared via OSSEs with another approach proposed by Gao and Stensrud (2012) that modifies the reflectivity observation operator so that the involvement of the hydrometeor state variables in the operator is temperature dependent, a treatment that they refer to as ''hydrometeor classification.''

Simulated radial velocity and reflectivity observations are assimilated every 5 min over a 60-min period for a simulated classic supercell storm. Three DA experiments are performed using 3DVar with invariant hydrometeor background error profiles (CTRL), with an additional hydrometeor classification treatment in the reflectivity observation operator (3DVarHC), and with the new temperature-dependent background error profiles and the original reflectivity operator (3DVarTD). The analyzed fields after the first 3DVar analysis and at the end of 1-h DA cycles are examined, together with the RMSEs of model state variables through the DA cycles. Major conclusions are summarized as follows:

1) All experiments are able to produce total reflectivity analyses that fit the truth reflectivity reasonably well. This is not surprising since reflectivity is observed and directly assimilated by the 3DVar. In contrast, significant differences are found with the analyzed hydrometeor fields.
2) When using constant background errors for the hydrometeors in CTRL, unphysical hydrometeor analyses are produced, including the presence of snow at the ground level for this summer storm. Wet snow below the freezing level is seriously overestimated because of its larger backscattering coefficient than rainwater and hail in the reflectivity observation operator. Dry snow at the high levels is seriously underestimated because of its smaller backscattering coefficient and the analysis of rainwater at the high levels.
3) In 3DVarHC, by employing temperature dependence of the reflectivity operator, unphysical analysis increment of rainwater above the −5°C level and of snow below the 5°C level cannot be directly produced from the reflectivity observation. However, because of the homogeneous vertical background error correlation used, the analysis increment of the rainwater is unphysically spread to the high levels and the analysis increment of snow is unphysically spread to the low levels. In addition, the exclusion of hail in the observation operator below the 5°C level leads to underestimated hail at the low levels.
4) When using the newly introduced temperature-dependent background error profiles, unphysical hydrometeor increments produced from reflectivity observations and unphysical vertical spreading when using homogenous background errors are much reduced. The analysis of snow mixing ratio is improved most over both CTRL and 3DVarHC.

Further improvement may be possible when the background error profiles of the hydrometeors are obtained statistically, from for example convective-scale model forecasts using a procedure similar to the NMC method. The error statistics should be calculated using data from precipitation regions only, and the statistics should be stratified according to temperature, and may need to consider other factors such as precipitation cycles. This can be a topic for future study. We also note that even with the procedure proposed in this study, the 3DVar system used in this study for hydrometeor analysis is univariate for the hydrometeors and does not fully utilize model equation constraints. Significant improvement is expected when ensemble-derived flow-dependent multivariate ensemble covariances are introduced into the variational framework, to formulate a hybrid ensemble–variational system. However, even in such a system, a proper and best possible treatment of the static background error covariance is still desirable. In fact, the proposed temperature-dependent error profiles are used in a recent 3DVar, En3DVar (ensemble 3DVar), and EnKF intercomparison study reported in Kong et al. (2018).

Acknowledgments. This research was primarily supported by the NOAA Warn-on-Forecast (WoF) Grant NA160AR4320115. The second author was also supported by NSF Grants AGS-0941491 and AGS-1046171. Computational resources of the Oklahoma Supercomputing Center for Research and Education (OSCER), and the NSF Xsede Supercomputing Centers were used.

REFERENCES

Aksoy, A., D. C. Dowell, and C. Snyder, 2009: A multicase comparative assessment of the ensemble Kalman filter for assimilation of radar observations. Part I: Storm-scale analyses. *Mon. Wea. Rev.*, **137**, 1805–1824, https://doi.org/10.1175/2008MWR2691.1.

——, ——, and ——, 2010: A multicase comparative assessment of the ensemble Kalman filter for assimilation of radar observations. Part II: Short-range ensemble forecasts. *Mon. Wea. Rev.*, **138**, 1273–1292, https://doi.org/10.1175/2009MWR3086.1.

Albers, S. C., J. A. McGinley, D. L. Birkenheuer, and J. R. Smart, 1996: The local analysis and prediction system (LAPS): Analyses of clouds, precipitation, and temperature. *Wea. Forecasting*, **11**, 273–287, https://doi.org/10.1175/1520-0434(1996)011<0273:TLAAPS>2.0.CO;2.

Gao, J., and D. J. Stensrud, 2012: Assimilation of reflectivity data in a convective-scale, cycled 3DVAR framework with hydrometeor classification. *J. Atmos. Sci.*, **69**, 1054–1065, https://doi.org/10.1175/JAS-D-11-0162.1.

——, M. Xue, K. Brewster, and K. K. Droegemeier, 2004: A three-dimensional variational data analysis method with recursive filter for Doppler radars. *J. Atmos. Oceanic Technol.*, **21**, 457–469, https://doi.org/10.1175/1520-0426(2004)021<0457:ATVDAM>2.0.CO;2.

Hamill, T. M., and C. Snyder, 2000: A hybrid ensemble Kalman filter–3D variational analysis scheme. *Mon. Wea. Rev.*, **128**, 2905–2919, https://doi.org/10.1175/1520-0493(2000)128<2905:AHEKFV>2.0.CO;2.

Houtekamer, P. L., and H. L. Mitchell, 1998: Data assimilation using an ensemble Kalman filter technique. *Mon. Wea. Rev.*, **126**, 796–811, https://doi.org/10.1175/1520-0493(1998)126<0796:DAUAEK>2.0.CO;2.

——, ——, and X. Deng, 2009: Model error representation in an operational ensemble Kalman filter. *Mon. Wea. Rev.*, **137**, 2126–2143, https://doi.org/10.1175/2008MWR2737.1.

Hu, M., M. Xue, and K. Brewster, 2006: 3DVAR and cloud analysis with WSR-88D level-II data for the prediction of Fort Worth tornadic thunderstorms. Part I: Cloud analysis and its impact. *Mon. Wea. Rev.*, **134**, 675–698, https://doi.org/10.1175/MWR3092.1.

Jung, Y. S., G. F. Zhang, and M. Xue, 2008a: Assimilation of simulated polarimetric radar data for a convective storm using the ensemble Kalman filter. Part I: Observation operators for reflectivity and polarimetric variables. *Mon. Wea. Rev.*, **136**, 2228–2245, https://doi.org/10.1175/2007MWR2083.1.

——, M. Xue, G. F. Zhang, and J. M. Straka, 2008b: Assimilation of simulated polarimetric radar data for a convective storm using the ensemble Kalman filter. Part II: Impact of polarimetric data on storm analysis. *Mon. Wea. Rev.*, **136**, 2246–2260, https://doi.org/10.1175/2007MWR2288.1.

Kain, J. S., and Coauthors, 2010: Assessing advances in the assimilation of radar data and other mesoscale observations within a collaborative forecasting–research environment. *Wea. Forecasting*, **25**, 1510–1521, https://doi.org/10.1175/2010WAF2222405.1.

Kong, R., M. Xue, and C. Liu, 2018: Development of a hybrid En3DVar data assimilation system and comparisons with 3DVar and EnKF for radar data assimilation with observing system simulation experiments. *Mon. Wea. Rev.*, **146**, 175–198, https://doi.org/10.1175/MWR-D-17-0164.1.

Lin, Y.-L., R. D. Farley, and H. D. Orville, 1983: Bulk parameterization of the snow field in a cloud model. *J. Climate Appl. Meteor.*, **22**, 1065–1092, https://doi.org/10.1175/1520-0450(1983)022<1065:BPOTSF>2.0.CO;2.

Parrish, D. F., and J. C. Derber, 1992: The National Meteorological Center's spectral statistical-interpolation analysis system. *Mon. Wea. Rev.*, **120**, 1747–1763, https://doi.org/10.1175/1520-0493(1992)120<1747:TNMCSS>2.0.CO;2.

Smith, P. L., Jr., C. G. Myers, and H. D. Orville, 1975: Radar reflectivity factor calculations in numerical cloud models using bulk parameterization of precipitation processes. *J. Appl. Meteor.*, **14**, 1156–1165, https://doi.org/10.1175/1520-0450(1975)014<1156:RRFCIN>2.0.CO;2.

Sun, J., and N. A. Crook, 1997: Dynamical and microphysical retrieval from Doppler radar observations using a cloud model and its adjoint. Part I: Model development and simulated data experiments. *J. Atmos. Sci.*, **54**, 1642–1661, https://doi.org/10.1175/1520-0469(1997)054<1642:DAMRFD>2.0.CO;2.

——, and Coauthors, 2014: Use of NWP for nowcasting convective precipitation: Recent progress and challenges. *Bull. Amer. Meteor. Soc.*, **95**, 409–426, https://doi.org/10.1175/BAMS-D-11-00263.1.

Tong, M. J., and M. Xue, 2005: Ensemble Kalman filter assimilation of Doppler radar data with a compressible nonhydrostatic model: OSS experiments. *Mon. Wea. Rev.*, **133**, 1789–1807, https://doi.org/10.1175/MWR2898.1.

Wang, H., J. Sun, S. Fan, and X.-Y. Huang, 2013a: Indirect assimilation of radar reflectivity with WRF 3D-Var and its impact on prediction of four summertime convective events.

J. Appl. Meteor. Climatol., **52**, 889–902, https://doi.org/10.1175/JAMC-D-12-0120.1.

——, ——, X. Zhang, X.-Y. Huang, and T. Auligné, 2013b: Radar data assimilation with WRF 4D-Var. Part I: System development and preliminary testing. *Mon. Wea. Rev.*, **141**, 2224–2244, https://doi.org/10.1175/MWR-D-12-00168.1.

Xiao, Q., Y.-H. Kuo, J. Sun, W.-C. Lee, D. M. Barker, and E. Lim, 2007: An approach of radar reflectivity data assimilation and its assessment with the inland QPF of typhoon Rusa (2002) at landfall. *J. Appl. Meteor. Climatol.*, **46**, 14–22, https://doi.org/10.1175/JAM2439.1.

Xu, Q., 1996: Generalized adjoint for physical processes with parameterized discontinuities. Part I: Basic issues and heuristic examples. *J. Atmos. Sci.*, **53**, 1123–1142, https://doi.org/10.1175/1520-0469(1996)053<1123:GAFPPW>2.0.CO;2.

Xue, M., and Coauthors, 2001: The Advanced Regional Prediction System (ARPS)—A multi-scale nonhydrostatic atmospheric simulation and prediction tool. Part II: Model physics and applications. *Meteor. Atmos. Phys.*, **76**, 143–165, https://doi.org/10.1007/s007030170027.

——, D.-H. Wang, J.-D. Gao, K. Brewster, and K. K. Droegemeier, 2003: The Advanced Regional Prediction System (ARPS), storm-scale numerical weather prediction and data assimilation. *Meteor. Atmos. Phys.*, **82**, 139–170, https://doi.org/10.1007/s00703-001-0595-6.

——, M. J. Tong, and K. K. Droegemeier, 2006: An OSSE framework based on the ensemble square root Kalman filter for evaluating the impact of data from radar networks on thunderstorm analysis and forecasting. *J. Atmos. Oceanic Technol.*, **23**, 46–66, https://doi.org/10.1175/JTECH1835.1.